Progress In Electromagnetics Research M, Vol. 18, 103–117, 2011

RADIATED EM FIELDS FROM A ROTATING CURRENT-CARRYING CIRCULAR CYLINDER: 2-DIMENSIONAL NUMERICAL SIMULATION

M. Ho

Department of Electronic Engineering
WuFeng University, Taiwan

F.-S. Lai

Department of Security Technology and Management
WuFeng University, Taiwan

Y.-H. Chen and W.-C. Lin

Department of Fire Science, WuFeng University, Taiwan

Abstract—The radiated electromagnetic (EM) fields from a rotating current-carrying circular cylinder were numerically simulated in two dimensions using the method of characteristics (MOC), and the numerical results were presented in this paper. To overcome the difficulty of the grid cell distortion caused by the rotating cylinder, the passing center swing back grids (PCSBG) technique is employed in collaboration of MOC in a modified O-type grid system. In order to have clear demonstration of radiated EM fields, the circular cylinder is set to be evenly divided in radial direction into an even number of slices that are made of perfect electric conductor (PEC) and nonelectric nonmagnetic material, alternatively. The surface current is assumed to have a Gaussian profile and to flow uniformly along the axial direction on the PEC surface. The radiated electric and magnetic fields around the cylinder were recorded as functions of time and reported along with the corresponding spectra which were obtained through proper Fourier transformation. Several field distributions over the whole computational space are also given.

Received 9 March 2011, Accepted 4 May 2011, Scheduled 12 May 2011
Corresponding author: Mingtsu Ho (homt@wfu.edu.tw).

1. INTRODUCTION

The analysis of electromagnetic radiation and scattering problems have been active topics of research because of theoretical interest and practical importance in both physics and engineering. Various techniques were designed to solve the reflected and scattered EM waves from slightly rough surfaces dated back to as early as 1951 [1] and 1963 [2]. In the presence of multiple objects the theoretical derivation turns out to be so complex that various approaches, though equipped with simplified assumptions and approximation techniques, can hardly progress any further. The scattering EM problems become even more complicated when the object of interest is not stationary. The difficulty is not only theoretical but also numerical. If researchers can come up with any analytical solutions for such problems, the resultant equations would be not only nonlinear but in complicated forms. Most of the time, such efforts typically end up in vain. Since the 1970s, many researchers have been making efforts in the study of scattered EM waves from uniformly moving or vibrating mirrors; some developed various theories while others worked on numerical solutions [3–9]. It is obvious that the role of numerical techniques becomes more and more important because many nonlinear and intricate problems can be numerically solved as well as because of the tremendous advance of computing power in both hardware and algorithm. The advance in computing power promises researchers to tackle difficult problems with complex structure. The computational results can hence provide researchers better understanding of detailed phenomena.

In numerical simulation, due to the movement of the targeted object, the shapes of grid cells adjacent to the moving object become time dependent. Grid cells can be changed in size and form and/or eliminated from the grid system; for some cases new cells can also be introduced into the grid system simultaneously. In [6], Harfoush et al. numerically simulated the EM scattering problem around the fundamental frequency using the finite-difference time-domain (FDTD) technique where the incident electric field was linearly interpolated whenever the moving boundary moves away from the grid point. It is reported that the elimination of already-existing cells and the addition of new cells can be taken care of by the MOC approach. One of the basic differences between FDTD and MOC is the positioning of field components. FDTD defines the electric and magnetic field components at the cell corners in an interlacing fashion [10]; MOC places all field components at the center of grid cell. When cells are gradually eliminated or added, the change does not affect the fact that all field variables are located at each cell's centroid. MOC evaluates

the flux change within each cell including the fractional ones all the time. Meanwhile, MOC adjusts the time step sizes of those fractional cells since the numerical time step for each cell is dependent on the grid size. It is shown that MOC yields results which are compatible with data generated by the FDTD technique [11] and in good agreement with the theoretical values when EM fields reflected from a traveling and/or vibrating perfect surface [12]. Also, MOC produces reasonable trends in the following cases: the effects of medium conductivity on the propagation of EM pulse onto conducting dielectric half space [13] and the propagation of EM pulse through lossless non-uniform dielectric slab [14].

In the case where object is rotating grid cells around object are twisted so badly that the numerical scheme is no longer applicable. To overcome this difficulty, thanks to the nature of MOC, the PCSBG technique was proposed in coalition with MOC [15, 16]. MOC with the aid of PCSBG was demonstrated to generate reasonable computational results in the scattered EM fields from rotating circular cylinder under the illumination of plane Gaussian EM pulse [17].

The main purpose of this paper is to observe, through the application of MOC combined with PCSBG to the solutions of Maxwell's equations, the EM fields radiated from a circular rotating cylinder on whose PEC portions surface currents are numerically set to flow. Both electric and magnetic fields around the cylinder are recorded as functions of time. The corresponding frequency-domain information becomes available via the use of Fourier transform. This paper is organized as follows: the numerical formulation and the boundary condition treatment of the problem are presented in Section 2; Section 3 illustrates the idea of the PCSBG technique; Section 4 defines the problem with the locations of the sampling points and the modified O-type grid system; the description of how the divided circular cylinder was arranged and the specifications of surface current are also given; Section 5 demonstrates the numerical results and is followed by the conclusion section.

2. GOVERNING EQUATIONS, SURFACE CURRENT AND BOUNDARY CONDITIONS

In the present problem, the EM fields are radiated from a rotating circular cylinder of infinite length and propagate in free space. Therefore, it can be fully described by the time-domain Maxwell's equations. MOC is an implicit approach numerically solving Maxwell curl equations in a curvilinear coordinate system. In free space, the

Maxwell's equations are

$$\frac{\partial \vec{B}}{\partial t} + \nabla \times \vec{E} = 0 \tag{1}$$

$$\frac{\partial \vec{D}}{\partial t} - \nabla \times \vec{H} = 0 \tag{2}$$

where $\vec{E}$ and $\vec{H}$ are the electric and magnetic field intensities, and $\vec{D}$ and $\vec{B}$ are the electric and magnetic flux densities. In the numerical model, the surface current on the rotating circular cylinder of infinite length has a Gaussian profile and is assumed to flow along the axial direction, namely the positive-z direction. Consequently, the electric components of the radiated EM fields are polarized in the z-direction, and the two magnetic field components are on the x-y plane. For the current task, a two-dimensional numerical formulation is adequate.

Because MOC directly approximates Maxwell's equations in a curvilinear coordinate system, the governing equations have to be rearranged in the form of Euler equation prior to the transform from the Cartesian system (t, x, y) to a curvilinear system (τ, ξ, η). After all these have been done, Maxwell's equations become

$$\frac{\partial Q}{\partial \tau} + \frac{\partial F}{\partial \xi} + \frac{\partial G}{\partial \eta} = 0 \tag{3}$$

where

$$q = [B_x \quad B_y \quad D_z]^T \tag{4}$$

$$f = [0 \quad -E_z \quad -H_y]^T \tag{5}$$

$$g = [E_z \quad 0 \quad H_x]^T \tag{6}$$

$$Q = Jq,\ F = Jf,\ G = Jg. \tag{7}$$

In the above equation, the symbol J is the Jacobian of the inverse transformation and defined as

$$J = \det \left| \frac{\partial(x, y)}{\partial(\xi, \eta)} \right|. \tag{8}$$

With the definition of the central difference scheme in mind,

$$\delta_k(\phi) = (\phi)_{k+\frac{1}{2}} - (\phi)_{k-\frac{1}{2}}, \tag{9}$$

the numerical formulation starts with the application of the central difference operator to (3). In (9), the symbol (ϕ) stands for the variable vector F or G corresponding to the subscript (k) representing the cell index along either ξ- or η-direction in the curvilinear coordinate system. Moreover, that the cell index (k) designates the centroid of

grid cell is being understood. The one-half index reveals the fact that MOC solves Maxwell's equations by evaluating flux across the interface between cells. By applying the central difference scheme (9) to (3), one obtains

$$\frac{Q^{n+1} - Q^n}{\Delta\tau} + \frac{\delta_i F}{\Delta\xi} + \frac{\delta_j G}{\Delta\eta} = 0. \tag{10}$$

Note that the finite difference symbol (Δ) has been applied to time and space. On vector Q the superscripts $(n+1)$ and (n) represent the two successive time levels; the first term therefore designates the approximation of the temporal derivative of vector Q. MOC solves the system of linear equations through the incorporation with the flux vector splitting technique and the lower-upper approximate factorization scheme.

The z-directed currents on the infinite, circular PEC cylinder surface are set to have a Gaussian profile with a peak value of one as in Figure 1(a). The Gaussian envelop has a width of $T = 0.2$ ns measured from the center to the point having the value of $e^{-0.5}$ and a cut-off level at 100 dB for practical reasons. The corresponding spectrum was obtained through Fourier transform and plotted in Figure 1(b) where the highest frequency content locates at about 3.8 GHz.

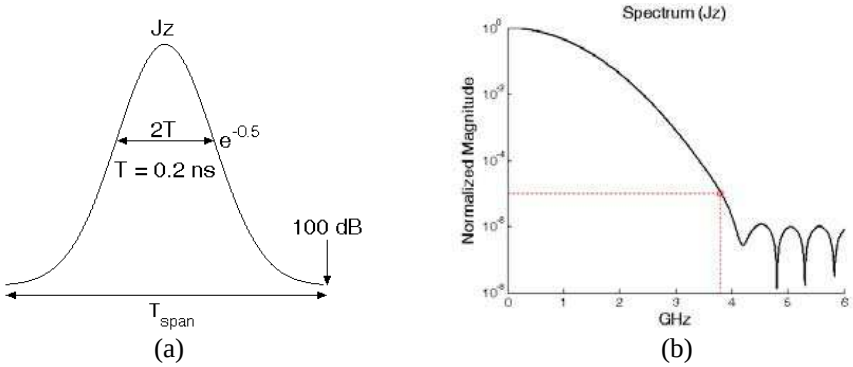

Figure 1. (a) Definition of the surface current (not to scale) and (b) its spectrum.

In the numerical model, there are two types of boundary conditions: one is on the cylinder PEC surface, and the other is on the truncated computational boundary. Given the surface currents (J_z), the boundary conditions at any point on the PEC surface can be

derived from the following

$$\hat{n} \times \vec{H} = 2J_z \tag{11}$$

$$\hat{n} \cdot \vec{B} = 0 \tag{12}$$

$$\hat{n} \times \vec{E} = 0 \tag{13}$$

where $\hat{n}$ is the exterior normal vector of the grid on the cylinder surface. It is noted that (12) ensures no EM fields with the magnetic field being perpendicular to the surface that can be radiated from the cylinder and that the electric field intensity must be vanished on the PEC cylinder surface according to (13). The radiated EM fields are then in the transverse electric mode. Additionally, on the surface of the nonelectric and nonmagnetic portion of the rotating cylinder both electric and magnetic fields are set to be null in magnitude. At the most outer numerical boundary the proper boundary conditions are to guarantee that the outgoing EM fields keep propagating outward.

3. THE PASSING CENTER SWING BACK GRIDS TECHNIQUE

The idea of the PCSBG technique was proposed with the purpose of solving the cell distortion difficulty. It is based on the nature of MOC which defines all field components at the cell centroid. A sequence of plots is given in Figure 2 to explain how the PCSBG

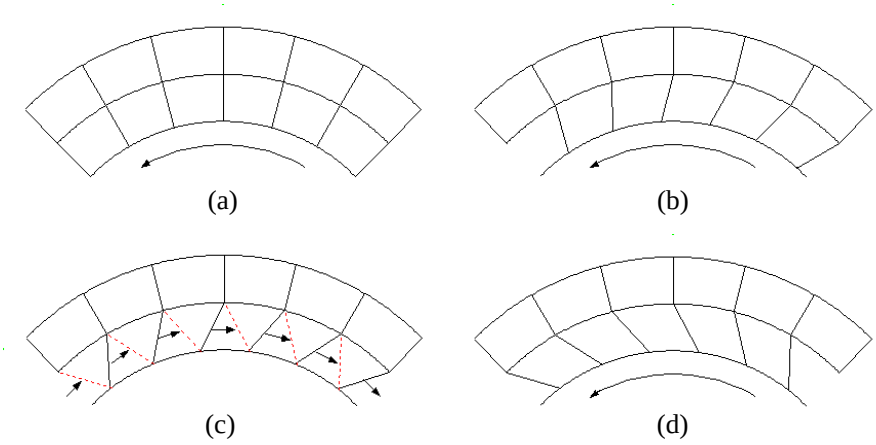

Figure 2. Schematic presentation of PCSBG: (a) Grids align at certain time instance; (b) grid lines are tilted; (c) grid lines pass the center point and are set to swing; (d) after the swing rotation continues.

design works. Each plot is composed of two layers of grids whose inner circle represents the cylinder. The layer of grids immediately next to cylinder is designated as the passing center swing back grids. They will suffer from deforming once the cylinder rotates since one side of these grids is attached to the cylinder. From the PCSBG layer outward are free space and grids are stationary throughout the process. Figures 2(a) and 2(b) show the grid lines are first at their alignment position at certain time instance and then twisted toward left due to the rotation of the cylinder (as indicated by arrow). Displayed in Figure 2(c), at the moment the grid lines are about to pass or at the cell center as depicted by the skewed black lines, and the PCSBG technique maneuvers them to swing back as depicted by the dotted red lines. The cylinder continues rotating after those grid lines has been reset by one grid backward as in Figure 2(d). Note that during the procedure the field variables are always defined at the cell centroid. Though MOC overcomes the difficulty caused by the rotating object, MOC cautiously book-keeps every change in the metrics terms of the swing back grids along with the exterior normal vector and the cell index of each grid on the cylinder surface. However, there is one exemption; the numerical time step of these swing back grids, in spite of the fact that it is grid size sensitive, remains constant even when the grid is twisted. It is because the grid size stays the same the whole time.

4. THE MODIFIED O-TYPE GRID AND THE PROBLEM SET UP

The present problem is characterized by a rotating circular cylinder carrying surface current, which results in the radiation of EM fields. The surface current is assumed to have a temporal Gaussian profile and to flow axially as described in the previous section. To numerically model the problem, the O-type grid system is a suitable candidate when a circular object is involved. Yet, regular O-type grid system is made of concentric circles. Even it is uniformly divided radially, grids turn into long thin trapezoids as radius increases and turn out to be unacceptable in modeling EM scattering related problems. To improve, the modified O-type grid is then proposed in which grid cells are doubled in number as radius grows to a certain size so that each grid remains within specific measurements in both dimensions. For clear illustration, a simplified version of the modified O-type grid is demonstrated in Figure 3, which is composed of three zones of grids. The cell numbers in each ring from zone to zone are 32 (black), 64 (red) and 128 (blue), respectively.

The surface currents flowing on the rotating cylinder have the

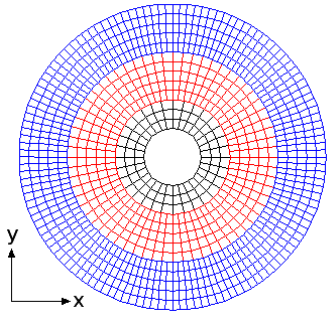

Figure 3. Modified O-type grid.

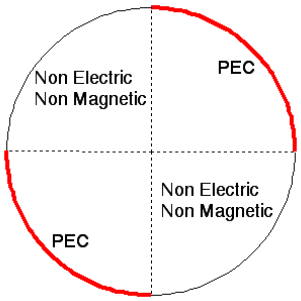

Figure 4. Cylinder has four sections.

previously defined Gaussian profile with a temporal span of about $T_{\text{span}} = 1.92\,\text{ns}$ measured from end to end (cut-off points). Any point outside this range is set to be zero in magnitude. The angular frequency of the rotating cylinder is defined as the number of the revolved cycle within one T_{span}. For example, if the cylinder makes one complete rotation (360°) in one T_{span}, the angular frequency would be a little bit greater than one π per nanosecond. Under such arrangement, it is equivalent that the instantaneous velocity of any point on the cylinder surface would be about 1.1 times as fast as the speed of light. Though an impractical figure this would be, the chief objective of the current task stays intact. For simplification and with the previous definition at hand, henceforth the term "cycle" will be used to define the angular frequency of the rotating cylinder. For similar reasons, another term "section-cycle number" stands for the product of the section number and the cycle number. The section-cycle number is eight, for instance, if a four-section cylinder rotates at 2 cycles.

Figure 4 illustrates a cylinder divided into four sections. For the purpose of clear demonstrating the effects of radiated EM fields from the rotating circular cylinder, these sections are assumed to be made of PEC and nonelectric nonmagnetic material, alternatively. In addition, there are eight sampling points located around at about 28.75 cm away from the cylinder surface. And they are equally spaced by 45° started from the x-axis (0°).

5. NUMERICAL RESULTS

The modified O-type grid system employed in the numerical model is composed of two portions: a cylinder in the center with a radius

of 10 cm and another 60 cm for the free space. There are three zones of grid outside the cylinder and 176 layers of grid in total. The grid number in each layer is doubling up from 336 (inner zone) to 1344 (outer zone). The grid density, in the units of grids per meter, ranges from 275 to 550 circumferentially and from 250 to 530 radially. The surface current is set to start out from zero in magnitude and takes 1 ns to reach the peak value. Remember that the time measured from the peak to the cut-off is 0.96 ns. The cylinder may be divided into two, four, or eight sections and may rotate at one, two, or four cycles.

Figure 5 shows two sets of field distribution taken at 1.6 ns where cylinders were severed into two halves and four quarters and may be at rest or rotate. Figures 5(a) and 5(e) are the radiated z-directed electric fields (E_z) from two stationary PEC cylinders. With close observations of these two radiated E_z distribution patterns, it is pointed out that E_z are wrapped around the cylinder in both cases and that E_z are super-positioned in the latter case. Figures 5(b) through 5(d) are respectively E_z, the x- and y-components of the magnetic field (H_x and H_y) when the two-section cylinder rotating at 4 cycles. And Figures 5(f) through 5(h) are for the four-section cylinder at 2 cycles. The followings are clearly shown: E_z forms a single-whirl pattern in

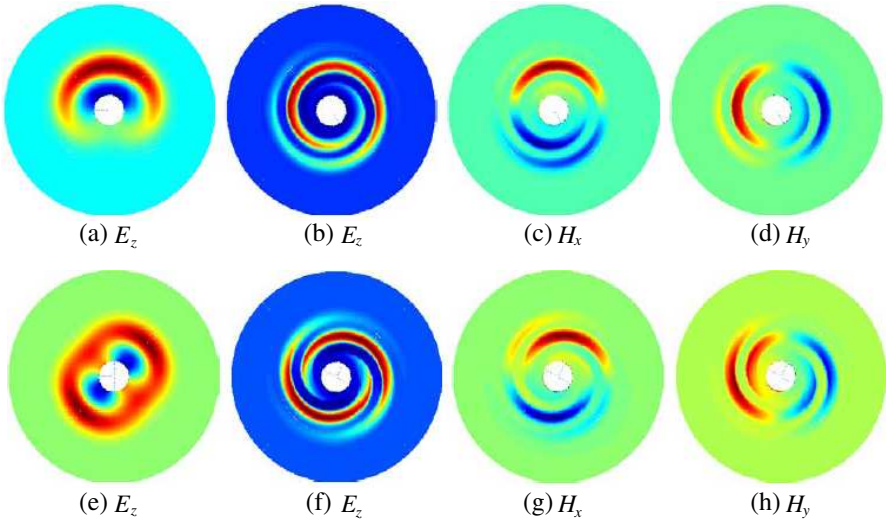

Figure 5. Field distributions over the whole computational domain at 1.6 ns. A two-section cylinder is (a) stationary and (b)–(d) rotating at 4 cycles. A four-section cylinder is (e) stationary and (f)–(h) rotating at 2 cycles. (background: zero; red: positive; blue: negative).

Figure 5(b) and a double-whirl pattern in Figure 5(f); there is no H_x in the x-direction in Figures 5(c) and 5(g), nor H_y in the y-direction in Figures 5(d) and 5(h); H_x and H_y in these two groups of plots bear similar patterns but differ in magnitude because they have same section-cycle numbers.

The radiated electric fields from various stationary cylinders, solid or severed, were recorded and displayed. Due to the symmetry, when the electric fields sampled at different points are alike, only one will be shown with remarks. For instance, eight lines coincide in the cases of solid cylinder and eight-section cylinder as in Figure 6(a). They are different in strength by a factor of about two. For a four-section cylinder there are three groups of lines as in Figure 6(b) and for a two-section cylinder five groups as in Figure 6(c). It is noticed that the relative strength and the location of primary lobe reveal information regarding the orientation of observer. Note also that the solid lines in three plots are identical as the result of geometric symmetry and field superposition. The corresponding normalized spectra were given in Figure 7. In Figure 7(a) the spectrum of surface current was included as a reference, and only the line of solid cylinder was shown since it is

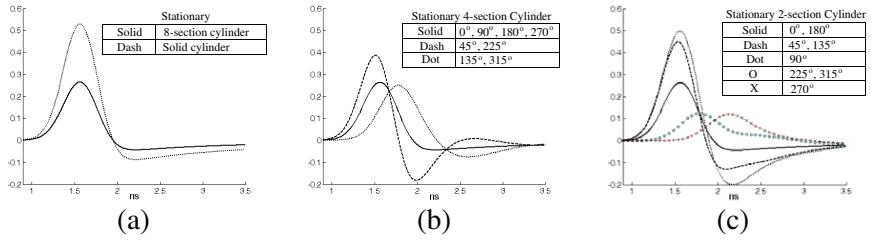

Figure 6. Radiated electric fields around stationary cylinders. (a) Solid and eight-section cylinders, (b) four-section cylinder, (c) two-section cylinder.

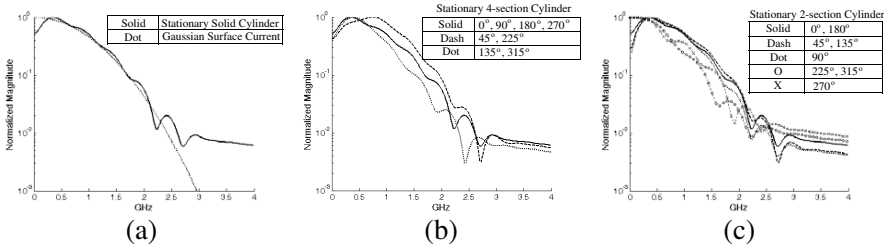

Figure 7. Spectra corresponding to the plots in Figure 6.

indistinguishable from that of eight-section cylinder. It is observed from Figures 7(b) and 7(c) that when the observer faces, fully or partially, the PEC portion, the spectrum of the radiated electric fields has lower level at DC and that those on the hind side have maxima ranging from DC up to about 0.3 GHz.

To investigate the effects of the rotation of cylinder on the radiated electric fields and spectra, the following efforts were made. The radiated electric fields from a two-section cylinder rotating at 4 cycles, whose radiated EM field patterns at 1.6 ns were shown in Figures 5(b)–(d), were recorded and illustrated in Figure 8(a) and their corresponding spectra in Figure 8(b). For clear illustration only four of eight different lines were plotted. A similar arrangement for a four-section cylinder rotating at 2 cycles, whose radiated EM field distributions at 1.6 ns were shown in Figures 5(e)–(h), was made and summarized in Figures 9(a) and 9(b). Unlike the preceding case, eight lines fall into four pairs as indicated in Figure 9(a). With close observations on the electric fields, it is shown, except the twin-lines in the latter case, that two sets of lines share similar behavior because the two section-cycle numbers are identical. On the spectra, though not very clearly, the separation between two successive minima is about 2 GHz in Figure 8(b), and that in Figure 9(b) is about 4 GHz.

Further efforts were made in the following two cases with identical section-cycle number: a four-section rotates at 4 cycles, and an eight-section rotates at 2 cycles. The numerical results were summarized in Figures 10 and 11. From the synchronous viewpoint, regardless the magnitude, the four electric fields in Figure 10(a) are almost equally spaced between two successive peaks while those in Figure 11(a) fall

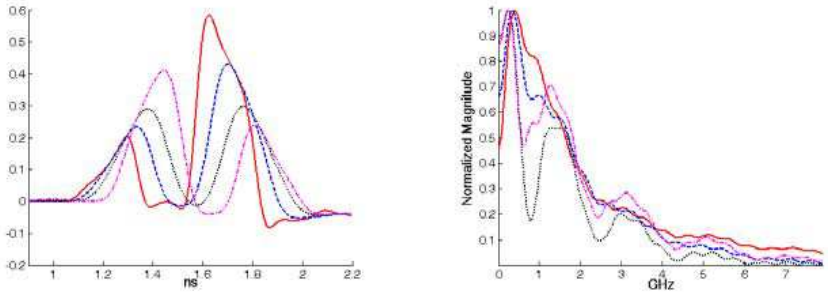

Figure 8. A two-section cylinder rotating at 4 cycles. (a) Radiated electric fields, (b) spectra. Solid: 180°; dash: 225°; dot: 270°; dash-dot: 315°.

into two groups separated by a distance twice as much. Though so, their spectra are nearly alike as depicted in Figures 10(b) and 11(b). Note that the secondary envelopes center at about 4 GHz in both cases. Finally, a set of radiated EM field patterns was given in Figure 12 for an eight-section cylinder rotating at various angular frequencies and at different instances of time. Compared with those in Figure 5, it is noticed that the more slices the cylinder is severed and/or the faster the cylinder rotates the thinner in shape the radiated fields are.

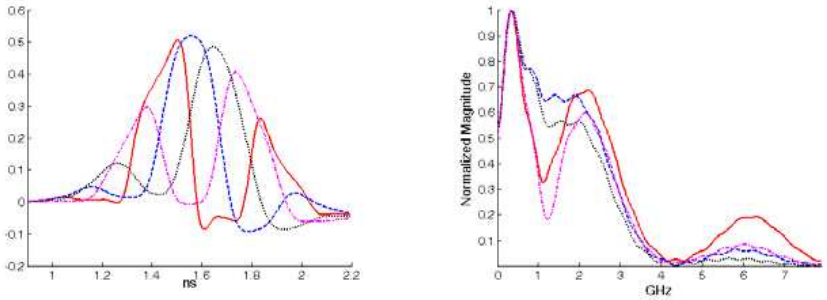

Figure 9. A four-section cylinder rotating at 2 cycles. (a) Radiated electric fields, (b) spectra. Solid: (0°, 180°); dash: (45°, 225°); dot: (90°, 270°); dash-dot: (135°, 315°).

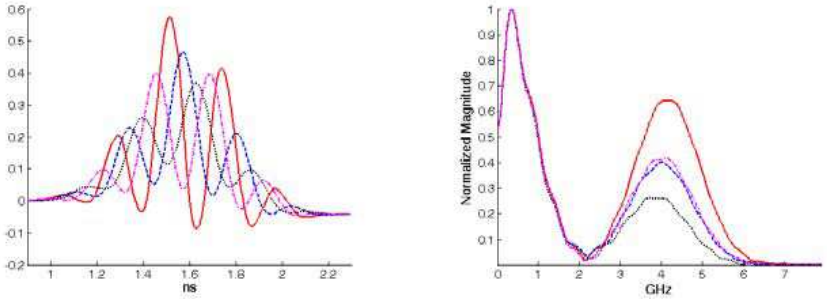

Figure 10. A four-section cylinder rotating at 4 cycles. (a) Radiated electric fields, (b) spectra. Solid: (0°, 180°); dash: (45°, 225°); dot: (90°, 270°); dash-dot: (135°, 315°).

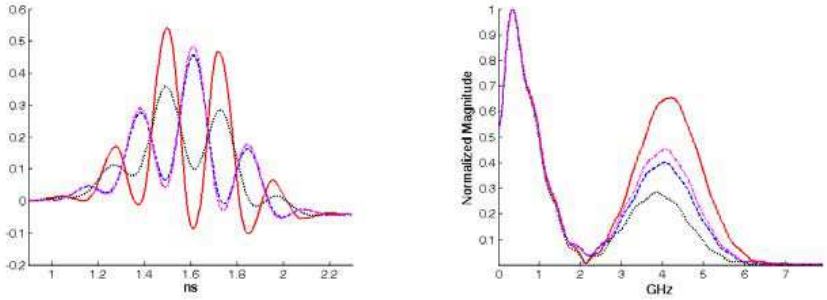

Figure 11. An eight-section cylinder rotating at 2 cycles. (a) Radiated electric fields, (b) spectra. Solid: (0°, 180°); dash: (45°, 225°); dot: (90°, 270°); dash-dot: (135°, 315°).

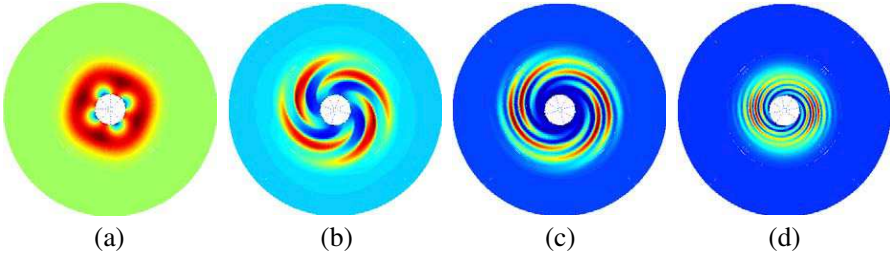

Figure 12. Field distributions of an eight-section cylinder that is (a) stationary at 1.3 ns, (b) rotating at 1 cycle at 1.6 ns, (c) rotating at 2 cycles at 1.6 ns, (d) rotating at 4 cycles at 1.07 ns. (background: zero; red: positive; blue: negative).

6. CONCLUSION

In this paper, it is shown that the method of characteristics incorporating with the passing center swing back grids technique overcomes the difficulty of grid distortion due to the rotation of object of interest while solving the Maxwell curl equations and produced feasible trends. The radiated electric fields are recorded and demonstrated along with the frequency-domain information. In the model the circular cylinder is divided into an even number of sections and rotates at various angular frequencies. Also given are several sets of two-dimensional plots of the electric fields and magnetic fields over the whole computational space. It is clearly illustrated that the radiated EM field patterns display whirl-like outline due to the

revolving movement of the current-carrying cylinder. The future work will be focused on simulating EM scattering problems involved rotating object in three dimensions.

REFERENCES

1. Rice, S. O., "Reflection of electromagnetic waves from slightly rough surface," *Commn. Pure Appl. Math.*, Vol. 4, 351–378, 1951.
2. Beckman, P. and A. Spizzichino, *The Scattering of Electromagnetic Waves from Rough Surfaces*, Pergamon, New York, 1963.
3. Baeva, T., S. Gordienko, and A. Pukhov, "Theory of high-order harmonic generation in relativistic laser interaction with overdense plasma," *Physical Review E*, Vol. 74, 046404, 2006.
4. Kleinman, R. E. and R. B. Mack, "Scattering by linearly vibrating objects," *IEEE Transactions on Antennas and Propagation*, Vol. 27, No. 3, 344–352, May 1979.
5. Cooper, J., "Scattering of electromagnetic fields by a moving boundary: The one-dimensional case," *IEEE Transactions on Antennas and Propagation*, Vol. 28, No. 6, 791–795, November 1980.
6. Harfoush, F., A. Taflove, and G. Kriegsmann, "A numerical technique for analyzing electromagnetic wave scattering from moving surfaces in one and two dimensions," *IEEE Transactions on Antennas and Propagation*, Vol. 37, No. 1, 55–63, January 1989.
7. Cooper, J., "Longtime behavior and energy growth for electromagnetic waves reflected by a moving boundary," *IEEE Transactions on Antennas and Propagation*, Vol. 41, No. 10, 1365–1370, October 1993.
8. Borkar, S. R. and R. F. H. Yang, "Scattering of electromagnetic waves from rough oscillating surface using spectral Fourier method," *IEEE Transactions on Antennas and Propagation*, Vol. 21, No. 5, 734–736, September 1973.
9. Van Bladel, J. and D. de Zutter, "Reflection from linearly vibrating objects: plane mirror at normal incidence," *IEEE Transactions on Antennas and Propagation*, Vol. 29, No. 4, 629–637, July 1981.
10. Yee, K., "Numerical solutions of initial boundary value problems involving Maxwell's equations in isotropic media," *IEEE Transactions on Antennas and Propagation*, Vol. 14, 302–307, 1966.
11. Donohoe, J. P., J. H. Beggs, and M. Ho, "Comparison of

finite-difference time-domain results for scattered EM fields: Yee algorithm vs. a characteristic based algorithm," *27th IEEE Southeastern Symposium on System Theory*, March 1995.

12. Ho, M., "Scattering of EM waves from traveling and/or vibrating perfect surface: Numerical simulation," *IEEE Transactions on Antennas and Propagation*, Vol. 54, No. 1, 152–156, January 2006.
13. Ho, M. and F.-S. Lai, "Effects of medium conductivity on electromagnetic pulse propagation onto dielectric half space: One-dimensional simulation using characteristic-based method," *Journal of Electromagnetic Waves and Applications*, Vol. 21, No. 13, 1773–1785, 2007.
14. Ho, M., F.-S. Lai, S.-W. Tan, and P.-W. Chen, "Numerical simulation of propagation of EM pulse through lossless non-uniform dielectric slab using characteristic-based method," *Progress In Electromagnetic Research*, Vol. 81, 197–212, 2008.
15. Ho, M., "Simulation of scattered fields from rotating cylinder in 2D: Under illumination of TE and TM Gaussian pulses," *PIERS Proceedings*, 1646–1651, Moscow, Russia, August 18–21, 2009.
16. Ho, M., "Numerically solving scattered electromagnetic fields from rotating objects using passing center swing back grid technique: A proposal," *Journal of Electromagnetic Waves and Applications*, Vol. 23, Nos. 2–3, 389–394, 2009.
17. Ho, M., "Simulation of scattered EM fields from rotating cylinder using passing center swing back grids technique in two dimensions," *Progress In Electromagnetic Research*, Vol. 92, 79–90, 2009.